Selective lanthanide distribution within a comprehensive series of heterometallic [LnPr] complexes

David Aguilà,[a] Verónica Velasco,[a] Leoní A. Barrios,[a] Joan González-Fabra,[b] Carles Bo,[b,c] Simon J. Teat,[d] Olivier Roubeau[e] and Guillem Aromí[a]

[a] Departament de Química Inorgànica i Orgànica, Secció de Química Inorgànica, Universitat de Barcelona, Diagonal 645, 08028 Barcelona (Spain)

[b] Institute of Chemical Research of Catalonia (ICIQ), The Barcelona Institute of Science and Technology, Av. Països Catalans 16, 43007 Tarragona (Spain)

[c] Departament de Química Física i Inorgànica, Universitat Rovira i Virgili, Marcel·lí Domingo s/n, 43007 Tarragona (Spain)

[d] Advanced Light Source, Berkeley Laboratory, 1 Cyclotron Road, Berkeley, California 94720 (USA)

[e] Instituto de Ciencia de Materiales de Aragón (ICMA) CSIC and Universidad de Zaragoza, Plaza San Francisco s/n, 50009, Zaragoza (Spain)

ABSTRACT: The preparation of heterometallic, only lanthanide complexes is an extremely difficult synthetic challenge. Following a ligand-based strategy, a complete isostructural series of dinuclear heterometallic [LnPr] complexes has been synthesized and structurally characterized. The two different coordination sites featured in this molecular entity allow studying the preferences of the praseodymium ion for a specific position depending on the ionic radii of the accompanying lanthanide partner. The purity of each heterometallic moiety has been evaluated in the solid state and in solution by means of crystallographic and spectrometric methods, respectively, revealing the limits of this strategy for ions with similar sizes. DFT calculations have been carried out to support the experimental results, confirming the nature of the site-selective lanthanide distribution. The predictable selectivity of this system has been exploited to assess the magnetic properties of the [PrDy] and [PrLu] derivatives, showing that the origin of the slow dynamics observed in the former arises from the dysprosium ion.

INTRODUCTION

The design of molecular systems featuring lanthanide (Ln) ions is a worldwide-pursued research subject due to the exceptional physical properties exhibited by these types of materials.[1-4] Since 4f orbitals are particularly screened form external perturbations by the filled 5s and 5p shells, their corresponding electrons virtually exhibit the magnetic and spectroscopic character of a free ion. This allows, for example, Ln ions to preserve their orbital momentum practically unquenched (only partially removed by the ligand field created in the coordination environment) or to produce a well-defined distribution of the electronic levels, deriving in sharp and easily identifiable 4f-4f transitions. These peculiarities permit to exploit Ln-based molecular systems in a wide range of applications such as devices for light-emitting diodes,[5] agents for optical and magnetic resonance imagining,[6] materials for magnetic refrigeration[7] or molecular-based systems

for information storage and processing.[8] In particular, the influence of Ln-based materials in molecular magnetism raised notably in the last years since Ishikawa and coworkers observed slow relaxation of the magnetization in a mononuclear $(Bu_4N)[Ln(phthalocyanine)_2]$ complex (Ln = Dy, Tb).[9] In fact, this area has recently reached one of its most relevant achievements with the discovery of a mononuclear dysprosium compound featuring such molecular-magnet behavior at almost liquid nitrogen temperature.[10] Considering the potential behind these materials, several research groups started to exploit the possibility of encapsulating more than one type of Ln ion within a molecular system, with the aim of controlling the nature of their metallic sites. These types of heterometallic moieties are particularly interesting since materials featuring combinations of different lanthanide ions can enhance or modify their physical properties. For example, they allow driving higher upconversion efficiencies in luminescent systems,[11] or tuning the color and the brightness of its emission.[12] Another interest is that compounds featuring lanthanide ions that emit at different wavelengths may allow contrast agents to cover both Vis and NIR regions.[13] Recently, the proposal of using lanthanide ions as the units of information for quantum computation (quantum bits or qubits)[14] raised also the interest for molecular systems featuring different Ln ions, since it allows the production of logical operators requiring more than one qubit.[15]

Despite the strong interest for accessing these type of 4f-4f' molecular systems, their production is not straightforward. Indeed, the shielding caused by the 5s and 5p electrons described above not only allows Ln ions to be protected from external perturbations but also leads them to behave chemically very similarly. Thus, coordination chemists have faced strong difficulties to develop synthetic methods to produce systems with predictably more than one type of Ln ion. One possibility stands on the sequential addition of the different lanthanide ions

through consecutive synthetic steps using a multidonor ligand[16] or by linking preformed building blocks.[17] On the other hand, the design of ligands featuring different encapsulating pockets allows the self-assembly and site-selective distribution of different type of Ln ions within molecules driven by their different ionic radii[18] through simple one-pot reactions. This strategy has allowed the production of triple-stranded heterometallic dinuclear[19] or trinuclear[20] helicates showing two different lanthanide ions selectively incorporated inside the cavities depending on their size with varying degrees of purity. Recently, the use of a rather simple quinolate ligand has produced also molecular systems featuring different metallic environments able to favor non-statistical distributions of different Ln ions among the various molecular locations.[21]

In the last years, we have developed a ligand-based strategy in order to achieve highly selective 4f-4f' dinuclear systems with a purity not observed in the previously reported heterometallic compounds.[15] By synthesizing the asymmetric H_3L ligand (H_3L = 6-(3-oxo-3-(2-hydroxyphenyl)propionyl)pyridine-2-carboxylic acid), a complete quasi-isostructural series of homometallic [LnLn] dinuclear compounds featuring two distinct metallic environments were initially synthesized (Scheme 1).[22] The flexibility of the system allowed to introduce any Ln^{III} ion in the two available coordination sites 1 and 2 of the molecule. However, the Ln-O bond distances of Ln in site 1 were found to be systematically smaller than the ones observed in site 2. This feature prompted us to exploit the possibility of introducing two different lanthanide ions with different ionic radii in order to produce, predictably, [LnLn'] compounds. Following this strategy, pure heterometallic systems were obtained for Ln pairs of considerable different sizes, although the selectivity was found to be reduced in solution, in the absence of the terminal ligands of the molecular entity.[23]

We have studied in detail this molecular system and tested the limits of its performance by making a comprehensive series where only one of the two lanthanide ions was varied. In particular, we have combined the praseodymium ion (Pr^{III}) together with each of the existing Ln^{III} ions (except Pm^{III}), obtaining a complete isostructural series: (Hpy)[LnPr(HL)$_3$(NO$_3$)(py)(H$_2$O)] (py = pyridine, Ln = La (**1**), Ce (**2**), Pr (**3**), Nd (**4**), Sm (**5**), Eu (**6**), Gd (**7**), Tb (**8**), Dy (**9**), Ho (**10**), Er(**11**), Tm (**12**), Yb (**13**), Lu (**14**)) hereafter expressed as [LnPr].

Scheme 1. Schematic representation of the anionic complex in (Hpy)[LnLn'(HL)$_3$(NO$_3$)(py)(H$_2$O)], emphasizing the coordination modes of the ligands in the system and the different cavities produced in site 1 (blue) and site 2 (green) and the two possible heterometallic [LnPr] combinations (type A and B).
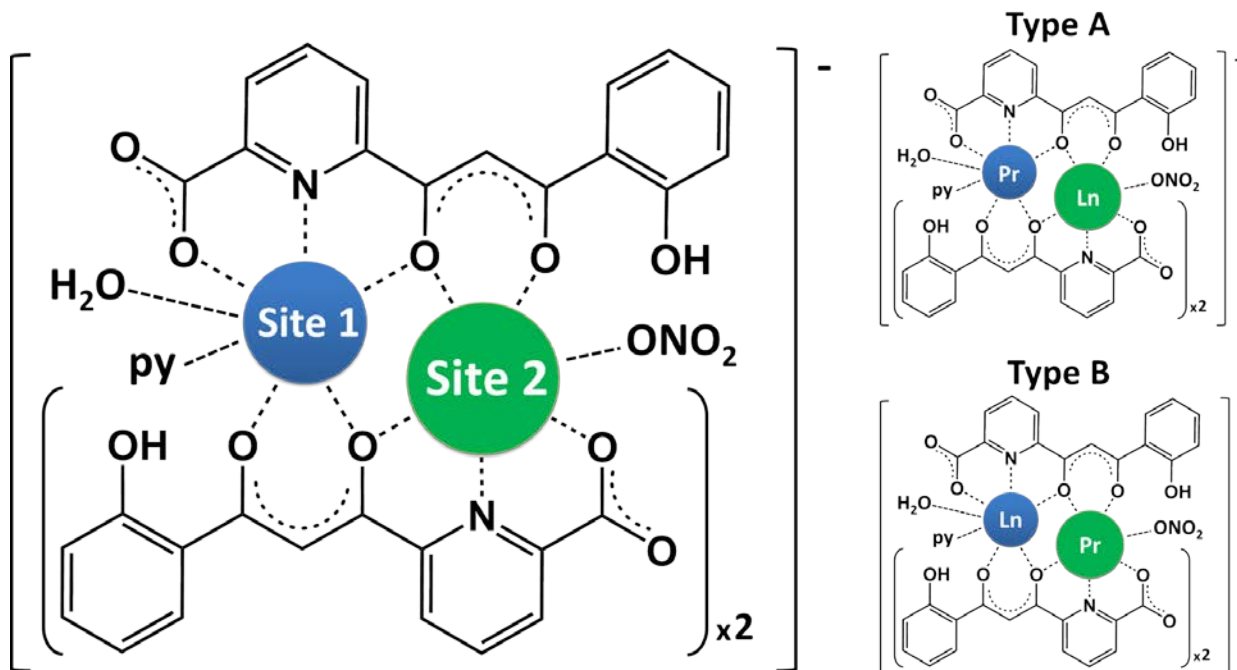
By means of X-ray crystallography, mass spectrometry and DFT calculations, we show here that the praseodymium cation can occupy a specific coordination site depending on the size of its accompanying Ln ion (Scheme 1). For Ln = La^{III} and Ce^{III}, the praseodymium cation prefers to be inserted in the smaller cavity 1 (Scheme 1, type A), although the selectivity is strongly limited given that the radii of these ions are not very different. In contrast, for the rest of the series (Ln = Nd^{III} to Lu^{III}) the positions are inversed and the praseodymium is encapsulated in site 2 (Scheme 1, type B). The purity of each compound has been studied by evaluating the Pr-O and Ln-O bond distances, as well as by exploring the different possible metallic combinations in the final refinement of the X-ray diffraction data. The new lanthanide series allows showing that the selectivity of this system, both in solution and in the solid state, is proportional to the difference between the ionic radii of Pr^{III} and that of its Ln^{III} partner (Δr). Moreover, the possibility of combining virtually any type of Ln^{III} together with Pr^{III} permits also to study a variety of properties. This enabled us, for example, to assess the magnetic behavior of the [DyPr] derivative and to explore its potential as single-molecule magnet. Moreover, the flexibility of the series allowed comparing its magnetic properties with [LuPr], where the praseodymium cation is the only paramagnetic center, thus elucidating the specific role of Pr^{III} and Dy^{III} in the slow relaxation of the magnetization.

EXPERIMENTAL SECTION

Synthesis. All reactions were performed under aerobic conditions, using the reagents as received unless otherwise indicated. The ligand 6-(3-oxo-3-(2-hydroxyphenyl)propionyl)pyridine-2-carboxylic acid (H$_3$L) was synthesized according to the

procedure described previously by us.[24] Each [LnPr] compound was synthesized following the approach reported for compounds [PrPr][22] and [SmPr],[23] varying the crystallization conditions.

(Hpy)[LaPr(HL)₃(NO₃)(py)(H₂O)] (1). A yellow solution of H_3L (30.0 mg, 0.105 mmol) in pyridine (10 mL) was added dropwise under stirring to a colorless solution of $Pr(NO_3)_3\cdot 6H_2O$ (15.2 mg, 0.035 mmol) and $La(NO_3)_3\cdot 6H_2O$ (15.2 mg, 0.035 mmol) in pyridine (10 mL). The resulting yellow solution was left under stirring for 2 h and layered with diethyl ether. After one week, yellow crystals of **1** were obtained (9 % yield). IR (KBr pellet): $\tilde{v}$ = 3400 (mb), 1618 (s), 1583 (s), 1559 (s), 1525 (s), 1461 (m), 1399 (s), 1382 (s), 1318 (m), 1297 (m), 1240 (w), 1206 (w), 1147 (w), 1120 (w), 1057 (w), 947 (w), 889 (w), 755 (w), 705 (w), 663 (w), 633 (w), 567 cm^{-1} (w). MS: m/z: 1130.53 $[LaPr(HL)_2(H_2L)]^+$, 1132.53 $[Pr_2(HL)_2(H_2L)]^+$. Elemental analysis calcd (%) for **1**·5.7H₂O·2py (based on 1:1 Pr/La): C 47.93, H 3.80, N 6.88; found: C 47.50, H 3.33, N 7.32.

(Hpy)[CePr(HL)₃(NO₃)(py)(H₂O)] (2). Compound **2** was obtained as orange crystals (17 % yield) following the same synthetic approach carried out for **1** but using $Ce(NO_3)_3\cdot 6H_2O$ (15.2 mg, 0.035 mmol) instead of $La(NO_3)_3\cdot 6H_2O$ and layering the final solution in toluene. IR (KBr pellet): $\tilde{v}$ = 3400 (mb), 1618 (s), 1583 (s), 1559 (s), 1525 (s), 1461 (m), 1399 (s), 1382 (s), 1318 (m), 1297 (m), 1240 (w), 1206 (w), 1147 (w), 1120 (w), 1057 (w), 947 (w), 889 (w), 755 (w), 705 (w), 663 (w), 633 (w), 567 cm^{-1} (w). MS: m/z: 1130.95 $[Ce_2(HL)_2(H_2L)]^+$, 1131.74 $[CePr(HL)_2(H_2L)]^+$, 1132.53 $[Pr_2(HL)_2(H_2L)]^+$. Elemental analysis calcd (%) for **2**·2.4 H₂O (based on 1:1 Pr/Ce): C 46.17, H 3.20, N 5.95; found: C 46.40, H 3.18, N 6.32.

(Hpy)[NdPr(HL)₃(NO₃)(py)(H₂O)] (4). Compound **4** was obtained as yellow crystals (22 % yield) following the same synthetic approach carried out for **1** but using $Nd(NO_3)_3\cdot 6H_2O$ (15.2 mg, 0.035 mmol) instead of $La(NO_3)_3\cdot 6H_2O$. IR (KBr pellet): $\tilde{v}$ = 3407 (mb), 1619 (s), 1584 (s),

1558 (s), 1525 (s), 1461 (m), 1399 (s), 1382 (s), 1323 (m), 1297 (m), 1240 (w), 1205 (w), 1147 (w), 1120 (w), 1056 (w), 947 (w), 889 (w), 754 (w), 705 (w), 663 (w), 633 (w), 567 cm^{-1} (w). MS: m/z: 1132.53 [Pr$_2$(HL)$_2$(H$_2$L)]$^+$, 1135.86 [NdPr(HL)$_2$(H$_2$L)]$^+$, 1139.19 [Nd$_2$(HL)$_2$(H$_2$L)]$^+$. Elemental analysis calcd (%) for **4**·5.5 H$_2$O (based on 1:1 Pr/Nd): C 44.84, H 3.49, N 5.70; found: C 44.25, H 2.78, N 6.28.

(Hpy)[EuPr(HL)$_3$(NO$_3$)(py)(H$_2$O)] (6). Compound **6** was obtained as yellow crystals (16 % yield) following the same synthetic approach carried out for **1** but using Eu(NO$_3$)$_3$·5H$_2$O (15.0 mg, 0.035 mmol) instead of La(NO$_3$)$_3$·6H$_2$O and layering the final solution in toluene. IR (KBr pellet): $\tilde{v}$ = 3410 (mb), 1618 (s), 1584 (s), 1558 (s), 1526 (s), 1463 (m), 1401 (s), 1384 (s), 1324 (m), 1298 (m), 1240 (w), 1208 (w), 1148 (w), 1121 (w), 1058 (w), 949 (w), 891 (w), 762 (w), 707 (w), 664 (w), 635 (w), 569 cm^{-1} (w).. MS: m/z: 1132.53 [Pr$_2$(HL)$_2$(H$_2$L)]$^+$, 1143.59 [EuPr(HL)$_2$(H$_2$L)]$^+$, 1154.64 [Eu$_2$(HL)$_2$(H$_2$L)]$^+$. Elemental analysis calcd (%) for **6**·4.1 H$_2$O (based on 1:1 Pr/Eu): C 45.41, H 3.34, N 5.78; found: C 44.93, H 2.85, N 5.74.

(Hpy)[GdPr(HL)$_3$(NO$_3$)(py)(H$_2$O)] (7). Compound **7** was obtained as yellow crystals (19 % yield) following the same synthetic approach carried out for **1** but using Gd(NO$_3$)$_3$·6H$_2$O (15.8 mg, 0.035 mmol) instead of La(NO$_3$)$_3$·6H$_2$O. IR (KBr pellet): $\tilde{v}$ = 3396 (mb), 1618 (s), 1584 (s), 1559 (s), 1527 (s), 1463 (m), 1400 (s), 1385 (s), 1324 (m), 1298 (m), 1240 (w), 1206 (w), 1148 (w), 1121 (w), 1058 (w), 949 (w), 891 (w), 759 (w), 707 (w), 664 (w), 635 (w), 568 cm^{-1} (w). MS: m/z: 1132.53 [Pr$_2$(HL)$_2$(H$_2$L)]$^+$, 1148.87 [GdPr(HL)$_2$(H$_2$L)]$^+$, 1165.21 [Gd$_2$(HL)$_2$(H$_2$L)]$^+$. Elemental analysis calcd (%) for **7**·4.1 H$_2$O (based on 1:1 Pr/Gd): C 45.24, H 3.33, N 5.76; found: C 44.96, H 3.00, N 5.64.

(Hpy)[TbPr(HL)$_3$(NO$_3$)(py)(H$_2$O)] (8). Compound **8** was obtained as yellow crystals (24 % yield) following the same synthetic approach carried out for **1** but using Tb(NO$_3$)$_3$·5H$_2$O (15.2

mg, 0.035 mmol) instead of La(NO$_3$)$_3$·6H$_2$O. IR (KBr pellet): $\tilde{v}$ = 3384 (mb), 1618 (s), 1584 (s), 1559 (s), 1526 (s), 1463 (m), 1397 (s), 1385 (s), 1324 (m), 1298 (m), 1240 (w), 1205 (w), 1147 (w), 1120 (w), 1058 (w), 949 (w), 890 (w), 755 (w), 706 (w), 664 (w), 635 (w), 567 cm^{-1} (w). MS: m/z: 1132.53 [Pr$_2$(HL)$_2$(H$_2$L)]$^+$, 1150.55 [TbPr(HL)$_2$(H$_2$L)]$^+$, 1168.56 [Tb$_2$(HL)$_2$(H$_2$L)]$^+$. Elemental analysis calcd (%) for **8**·3.3 H$_2$O (based on 1:1 Pr/Tb): C 45.64, H 3.25, N 5.81; found: C 45.07, H 2.67, N 6.05.

(Hpy)[DyPr(HL)$_3$(NO$_3$)(py)(H$_2$O)] (9). Compound **9** was obtained as yellow crystals (24 % yield) following the same synthetic approach carried out for **1** but using Dy(NO$_3$)$_3$·5H$_2$O (15.4 mg, 0.035 mmol) instead of La(NO$_3$)$_3$·6H$_2$O. IR (KBr pellet): $\tilde{v}$ = 3400 (mb), 1618 (s), 1584 (s), 1559 (s), 1527 (s), 1463 (m), 1400 (s), 1384 (s), 1325 (m), 1298 (m), 1240 (w), 1205 (w), 1147 (w), 1121 (w), 1059 (w), 950 (w), 891 (w), 759 (w), 707 (w), 664 (w), 635 (w), 569 cm^{-1} (w). MS: m/z: 1132.53 [Pr$_2$(HL)$_2$(H$_2$L)]$^+$, 1154.12 [DyPr(HL)$_2$(H$_2$L)]$^+$, 1175.71 [Dy$_2$(HL)$_2$(H$_2$L)]$^+$. Elemental analysis calcd (%) for **9**·4.5 (based on 1:1 Pr/Dy): C 44.86, H 3.35, N 5.71; found: C 44.54, H 3.01, N 5.62.

(Hpy)[HoPr(HL)$_3$(NO$_3$)(py)(H$_2$O)] (10). Compound **10** was obtained as yellow crystals (21 % yield) following the same synthetic approach carried out for **1** but using Ho(NO$_3$)$_3$·5H$_2$O (15.4 mg, 0.035 mmol) instead of La(NO$_3$)$_3$·6H$_2$O. IR (KBr pellet): $\tilde{v}$ = 3392 (mb), 1618 (s), 1584 (s), 1559 (s), 1526 (s), 1463 (m), 1400 (s), 1382 (s), 1324 (m), 1298 (m), 1239 (w), 1202 (w), 1147 (w), 1120 (w), 1058 (w), 950 (w), 891 (w), 755 (w), 706 (w), 664 (w), 635 (w), 568 cm^{-1} (w). MS: m/z: 1132.53 [Pr$_2$(HL)$_2$(H$_2$L)]$^+$, 1156.55 [HoPr(HL)$_2$(H$_2$L)]$^+$, 1180.57 [Ho$_2$(HL)$_2$(H$_2$L)]$^+$. Elemental analysis calcd (%) for **10**·4.4 H$_2$O (based on 1:1 Pr/Ho): C 44.84, H 3.34, N 5.70; found: C 44.42, H 2.89, N 5.80.

(Hpy)[ErPr(HL)₃(NO₃)(py)(H₂O)] (11). Compound **11** was obtained as orange crystals (20 % yield) following the same synthetic approach carried out for **1** but using $Er(NO_3)_3 \cdot 5H_2O$ (15.5 mg, 0.035 mmol) instead of $La(NO_3)_3 \cdot 6H_2O$. IR (KBr pellet): $\tilde{v}$ = 3398 (mb), 1618 (s), 1584 (s), 1559 (s), 1527 (s), 1464 (m), 1401 (s), 1385 (s), 1325 (m), 1299 (m), 1239 (w), 1203 (w), 1147 (w), 1121 (w), 1059 (w), 951 (w), 891 (w), 756 (w), 707 (w), 664 (w), 635 (w), 569 cm^{-1} (w). MS: m/z: 1132.53 $[Pr_2(HL)_2(H_2L)]^+$, 1158.58 $[ErPr(HL)_2(H_2L)]^+$, 1185.23 $[Er_2(HL)_2(H_2L)]^+$. Elemental analysis calcd (%) for **11**·4.7 H_2O (based on 1:1 Pr/Er): C 44.61, H 3.36, N 5.67; found: C 44.13, H 2.84, N 5.55.

(Hpy)[TmPr(HL)₃(NO₃)(py)(H₂O)] (12). Compound **12** was obtained as yellow crystals (20 % yield) following the same synthetic approach carried out for **1** but using $Tm(NO_3)_3 \cdot 5H_2O$ (15.6 mg, 0.035 mmol) instead of $La(NO_3)_3 \cdot 6H_2O$. IR (KBr pellet): $\tilde{v}$ = 3402 (mb), 1618 (s), 1584 (s), 1558 (s), 1528 (s), 1464 (m), 1402 (s), 1384 (s), 1325 (m), 1299 (m), 1239 (w), 1203 (w), 1148 (w), 1121 (w), 1059 (w), 951 (w), 891 (w), 758 (w), 707 (w), 664 (w), 636 (w), 569 cm^{-1} (w). MS: m/z: 1160.56 $[PrTm(HL)_2(H_2L)]^+$. Elemental analysis calcd (%) for **12**·4.8 H_2O (based on 1:1 Pr/Tm): C 44.50, H 3.37, N 5.66; found: C 43.87, H 2.73, N 5.72.

(Hpy)[YbPr(HL)₃(NO₃)(py)(H₂O)] (13). Compound **13** was obtained as yellow crystals (25 % yield) following the same synthetic approach carried out for **1** but using $Yb(NO_3)_3 \cdot 5H_2O$ (15.7 mg, 0.035 mmol) instead of $La(NO_3)_3 \cdot 6H_2O$. IR (KBr pellet): $\tilde{v}$ = 3412 (mb), 1618 (s), 1584 (s), 1558 (s), 1529 (s), 1463 (m), 1402 (s), 1384 (s), 1325 (m), 1300 (m), 1239 (w), 1204 (w), 1148 (w), 1121 (w), 1059 (w), 952 (w), 892 (w), 758 (w), 707 (w), 664 (w), 636 (w), 569 cm^{-1} (w). MS: m/z: 1164.66 $[PrYb(HL)_2(H_2L)]^+$. Elemental analysis calcd (%) for **13**·4.7 H_2O (based on 1:1 Pr/Yb): C 44.43, H 3.35, N 5.65; found: C 43.93, H 2.81, N 5.73.

(Hpy)[LuPr(HL)₃(NO₃)(py)(H₂O)] (14). Compound **14** was obtained as yellow crystals (10 % yield) following the same synthetic approach carried out for **1** but using $Lu(NO_3)_3 \cdot xH_2O$ (12.6 mg, 0.035 mmol) instead of $La(NO_3)_3 \cdot 6H_2O$. IR (KBr pellet): $\tilde{v}$ = 3406 (mb), 1618 (s), 1584 (s), 1558 (s), 1529 (s), 1464 (m), 1402 (s), 1384 (s), 1326 (m), 1300 (m), 1240 (w), 1202 (w), 1148 (w), 1121 (w), 1060 (w), 952 (w), 891 (w), 762 (w), 707 (w), 664 (w), 636 (w), 569 cm⁻¹ (w). MS: m/z: 1166.59 [LuPr(HL)₂(H₂L)]⁺. Elemental analysis calcd (%) for **14**·3.9 H_2O (based on 1:1 Pr/Lu): C 44.81, H 3.27, N 5.7; found: C 44.67, H 3.08, N 5.69.

Single-Crystal X-ray diffraction. Data for compounds **1**, **2**, **4**, **6**, **8**, **9**, **11**, **12**, and **13** were collected using a Bruker APEX II CCD diffractometer on the Advanced Light Source beamline 11.3.1 at Lawerence Berkeley National Laboratory, from a silicon 111 monochromator (λ = 0.7749 Å). Data for compounds **7**, **10** and **14** were collected on a Bruker APEX II QUAZAR diffractometer equipped with a microfocus multilayer monochromator with $Mo_{K\alpha}$ radiation (λ = 0.71073 Å). Data reduction and absorption corrections were performed by using SAINT and SADABS, respectively.[25] The structures were solved using SHELXT[26] and refined with full-matrix least-squares on F^2 by suing SHELXL-2014.[27] The heterometallic nature of the compounds was assessed by evaluating the agreement factors and the relative displacement parameters of the corresponding lanthanides considering the four possible combinations (LnLn', Ln'Ln, LnLn and Ln`Ln`), as summarized in Table S1 and S2.

Infrared Spectroscopy. IR spectra were recorded as KBr pellets in the range of 4000-400 cm⁻¹ by using a Thermo Nicolet Avatar 330 FT-IR spectrometer.

Mass Spectrometry. Positive-ion ESI mass spectrometry experiments were performed by using a LC/MSD-TOF (Agilent Technologies) with a dual source equipped with a lock spray for internal reference introduction, at the Unitat d'Espectrometria de Masses (SSR) from the

Universitat de Barcelona. Experimental parameters: capillary voltage 4 kV, gas temperature 325°C, nebulizing gas pressure 103.42 kPa, drying gas flow 7.0 L min^{-1} and fragmentor voltage 175-250 V. Internal reference masses were m/z 121.05087 (purine) or 922.00979 (HP-0921). Samples were dissolved in a mixture of MeOH/DMSO (µL) and introduced into the source by using a HPLC system (Agilent 110) with a mixture of H_2O/CH_3CN (1:1) as the eluent (200 µL min^{-1}).

Elemental Analysis. C, H, N analyses were performed by using a Thermo EA Flash 2000 (Thermo Scientific) analyser at the Centres Científics i Tecnològics from the Universitat de Barcelona (CCiT-UB).

Computational Details. All geometries were fully optimized using DFT based methods by employing the ADF program (Scientific Computing and Modelling ADF-2016, http://www.scm.com) The Becke [28] and Perdew [29] gradient-corrected exchange and correlation functionals (BP86), respectively, were used in the calculations. Also, the B3LYP functional was tested. [30] The ZORA [31] scalar relativistic Hamiltonian was employed together with a TZP basis set[31a] for carbon, oxygen, nitrogen and hydrogen atoms, and TZ2P basis set for metal atoms. In contrast to ZORA scalar relativistic approximation, relativistic Spin-Orbit were also carried out. The geometry optimizations were performed with the default numerical integration scheme of Becke. [32] Molecular geometries were optimized without constraints. Some counter measures to induce SCF convergence were included when B3LYP functional was used, namely level shift (0.15) and strong damping (density mixing step of 0.05). A data set collection of computational results is available in the ioChem-BD repository[33] and can be accessed via http://dx.doi.org/10.19061/iochem-bd-1-64.

Magnetic measurements. Magnetic measurements were performed on polycrystalline samples with a commercial magnetometer equipped with a SQUID sensor and a commercial Physical Properties Measurement System (PPMS), both hosted by the Physical Measurements Unit of the Servicio General de Apoyo a la Investigación-SAI, Universidad de Zaragoza. The diamagnetic contributions to the susceptibility were corrected using Pascal's constant tables. Direct current (*dc*) data were collected between 2 and 300 K with an applied field of 100 Oe. Alternating current (*ac*) data were collected with an applied *ac* field of 4 Oe oscillating at different frequencies in the range $0.1 \leq v \leq 10\ 000$ Hz. Data at variable temperatures were obtained with the PPMS set-up that allows to reach 10 kHz in frequency. Small variations between measurements done on the two set-ups may be ascribed to a lower sensibility as well as to the presence of a small remnant *dc* field for the latter.

RESULTS AND DISCUSSION

Synthesis. The compounds of the comprehensive series of dinuclear (Hpy)[LnPr(HL)$_3$(NO$_3$)(py)(H$_2$O)] ([LnPr]) complexes were obtained following the same synthetic procedure developed for the reported analogues [PrPr] and [SmPr].[22, 23] Thus, the stoichiometric amount of ligand H$_3$L was mixed in pyridine with equimolar amounts of Pr(NO$_3$)$_3$ and the corresponding Ln(NO$_3$)$_3$ salt. Slow diffusion of diethyl ether or toluene into the resulting reaction mixture allowed the formation of needle-type crystals that were collected and characterized. The molecular formula was confirmed by elemental analysis and single crystal X-ray diffraction, the latter also used to evaluate the heterometallic character of the compounds. As expected, the yields obtained (from 9 % for [LaPr] to 25 % for [YbPr]) were in agreement with the results previously reported for the analogous systems. Interestingly, this synthetic procedure

allowed obtaining for the first time a full series of compounds ([LnPr]) in the form of single crystals, in contrast to what is the case with the analogous [LnLn] series, for which compounds [LaLa] and [LuLu] were obtained as amorphous materials ([LaLa] crystallized only when tuning the pH of the medium).[22] This confirms the preference of this molecular architecture to encapsulate two lanthanides with different ionic radii, and its limitations when trying to gather two very big (La) or very small (Lu) ions.

Structural characterization. All compounds of the series, $(Hpy)[LnPr(HL)_3(NO_3)(py)(H_2O)]$ (**1** to **14**), are isostructural and crystallize in the monoclinic $P2_1/c$ space group. The asymmetric unit shows one [LnPr] molecule together with four molecules of pyridine. In some cases, the crystal lattice contains additional pyridine or water molecules (Table 1). The crystal structure shows one Ln and one Pr cation encapsulated by three doubly deprotonated HL ligands exhibiting two different orientations (Figures 1 and S1). This molecular architecture thus provides two different coordination sites, 1 and 2, composed by different chelating units derived from HL^{2-} (Scheme 1). Site 1 is formed by two diketonate (O,O) and one dipicolinate-like (O,N,O) groups, completing a coordination number (CN) of nine with one molecule of pyridine and one molecule of water. In contrast, for site 2, two dipicolinate-like and one diketonate pockets encapsulate the lanthanide ion, which exhibits CN of ten with the concurrence of a molecule of NO_3^- in a bidentate mode. The electroneutrality of the system is achieved with a molecule of pyridinium (Hpy), which interacts with one of the carboxylic groups of the molecule through hydrogen bonding (Figure S1).

Table 1. Crystallographic and refinement parameters for compounds **1-14**.

	1·4py·H₂O	**2·4py·H₂O**	**3·5py**	**4·4py·H₂O**	**5·4py·H₂O**	**6·4py·H₂O**	**7·5py**
formula	$C_{75}H_{62}LaN_{10}O_{20}Pr$	$C_{75}H_{62}CeN_{10}O_{20}Pr$	$C_{80}H_{65}N_{11}O_{19}Pr_2$	$C_{75}H_{62}N_{10}NdO_{20}Pr$	$C_{75}H_{62}N_{10}O_{20}PrSm$	$C_{75}H_{62}EuN_{10}O_{20}Pr$	$C_{80}H_{58}GdN_{11}O_{19}Pr$
FW [g mol⁻¹]	1703.16	1704.37	1766.25	1708.49	1712.59	1716.21	1775.53
λ [Å]	0.7749	0.7749	0.7749	0.7749	0.7749	0.7749	0.71073
T [K]	100	100	100	150	150	100	100
crystal system	monoclinic	monoclinic	monoclinic	monoclinic	monoclinic	monoclinic	monoclinic
space group	$P2_1/c$	$P2_1/c$	$P2_1/c$	$P2_1/c$	$P2_1/c$	$P2_1/c$	$P2_1/c$
a [Å]	14.944(2)	15.061(6)	14.907(3)	14.9637(11)	14.944(2)	14.923(2)	14.5062(4)
b [Å]	15.583(2)	15.636(6)	15.574(3)	15.6214(11)	15.664(2)	15.6485(8)	15.8238(5)
c [Å]	33.435(3)	32.925(11)	34.009(6)	32.655(2)	32.606(4)	32.395(7)	35.5880(10)
β [°]	110.735(4)	110.636(14)	111.316(8)	110.769(3)	110.857(5)	110.979(15)	113.196(2)
V [Å³]	7281.8(15)	7256(5)	7355(2)	7137.2(9)	7132.4(16)	7063.5(19)	7508.6(4)
Z	4	4	4	4	4	4	4
ρ_{calcd} [g cm⁻³]	1.554	1.560	1.595	1.590	1.595	1.614	1.571
μ [mm⁻¹]	1.644	1.701	1.734	1.840	1.964	2.049	1.598
indep. reflns. (R_{int})	9829 (0.0882)	9141 (0.0934)	22491 (0.0479)	18613 (0.0457)	10885 (0.0390)	19850 (0.0538)	19292 (0.0611)
restraints/ parameters	301/974	198/966	454/1063	265/1006	268/1009	266/1016	117/1044
GOF on F^2	1.104	1.044	1.160	1.201	1.157	1.016	1.137
R_1/wR_2 [$I>2\sigma(I)$]	0.0779/0.1744	0.0456/0.1061	0.0536/0.1302	0.0480/0.1126	0.0341/0.0837	0.0309/0.0708	0.0517/0.1320
R_1/wR_2 (all data)	0.1016/0.1864	0.0664/0.1162	0.0625/0.1364	0.0577/0.1176	0.0406/0.0879	0.0449/0.0769	0.0749/0.1551

	8·5py	**9·5py**	**10·5py**	**11·5py**	**12·5py**	**13·4py**	**14·5py**
formula	$C_{80}H_{65}N_{11}O_{19}PrTb$	$C_{80}H_{65}DyN_{11}O_{19}Pr$	$C_{80}H_{65}HoN_{11}O_{19}Pr$	$C_{80}H_{65}ErN_{11}O_{19}Pr$	$C_{80}H_{65}N_{11}O_{19}PrTm$	$C_{75}H_{60}N_{10}O_{19}PrYb$	$C_{80}H_{65}LuN_{11}O_{19}Pr$
MW [g mol⁻¹]	1784.26	1787.84	1790.27	1792.60	1794.27	1719.28	1800.31
wavelength [Å]	0.7749	0.7749	0.71073	0.7749	0.7749	0.7749	0.71073
T [K]	150	150	100	150	150	100	100
crystal system	monoclinic	monoclinic	monoclinic	monoclinic	monoclinic	monoclinic	monoclinic
space group	$P2_1/c$	$P2_1/c$	$P2_1/c$	$P2_1/c$	$P2_1/c$	$P2_1/c$	$P2_1/c$

|							
a [Å]	14.4957(10)	14.514(3)	14.5196(11)	14.466(3)	14.526(2)	14.5212(9)	14.4938(10)
b [Å]	15.8090(11)	15.799(3)	15.8819(11)	15.859(3)	15.823(2)	15.8174(10)	15.8951(11)
c [Å]	35.6637(19)	35.629(6)	35.375(2)	35.258(7)	35.410(3)	35.3296(19)	35.133(2)
β [°]	113.270(2)	113.034(6)	112.887(4)	112.39(3)	112.544(3)	112.064(2)	112.437(4)
V [Å^3]	7508.0(8)	7519(2)	7515.2(9)	7479(3)	7516.9(15)	7520.5(8)	7481.2(9)
Z	4	4	4	4	4	4	4
ρ_{calcd} [g cm^{-3}]	1.579	1.579	1.582	1.592	1.585	1.518	1.598
μ [mm^{-1}]	2.063	2.130	1.767	2.291	2.358	2.433	2.037
independent reflns (R_{int})	22891 (0.0737)	22901 (0.0746)	16627 (0.0554)	25995 (0.0527)	18623 (0.0864)	22829 (0.0611)	17157 (0.0619)
restraints/ parameters	140/991	703/1122	414/982	639/1052	714/1111	161/1034	287/998
GOF on F^2	1.039	1.060	1.117	1.118	1.037	1.130	1.070
R_1/wR_2 [$I>2\sigma(I)$]	0.0505/0.1280	0.0368/0.0882	0.0676/0.1549	0.0385/0.0992	0.0473/0.1138	0.0604/0.1449	0.0689/0.1503
R_1/wR_2 (all data)	0.0631/0.1351	0.0441/0.0916	0.0897/0.1650	0.0435/0.1026	0.0614/0.1207	0.0730/0.1492	0.0967/0.1621
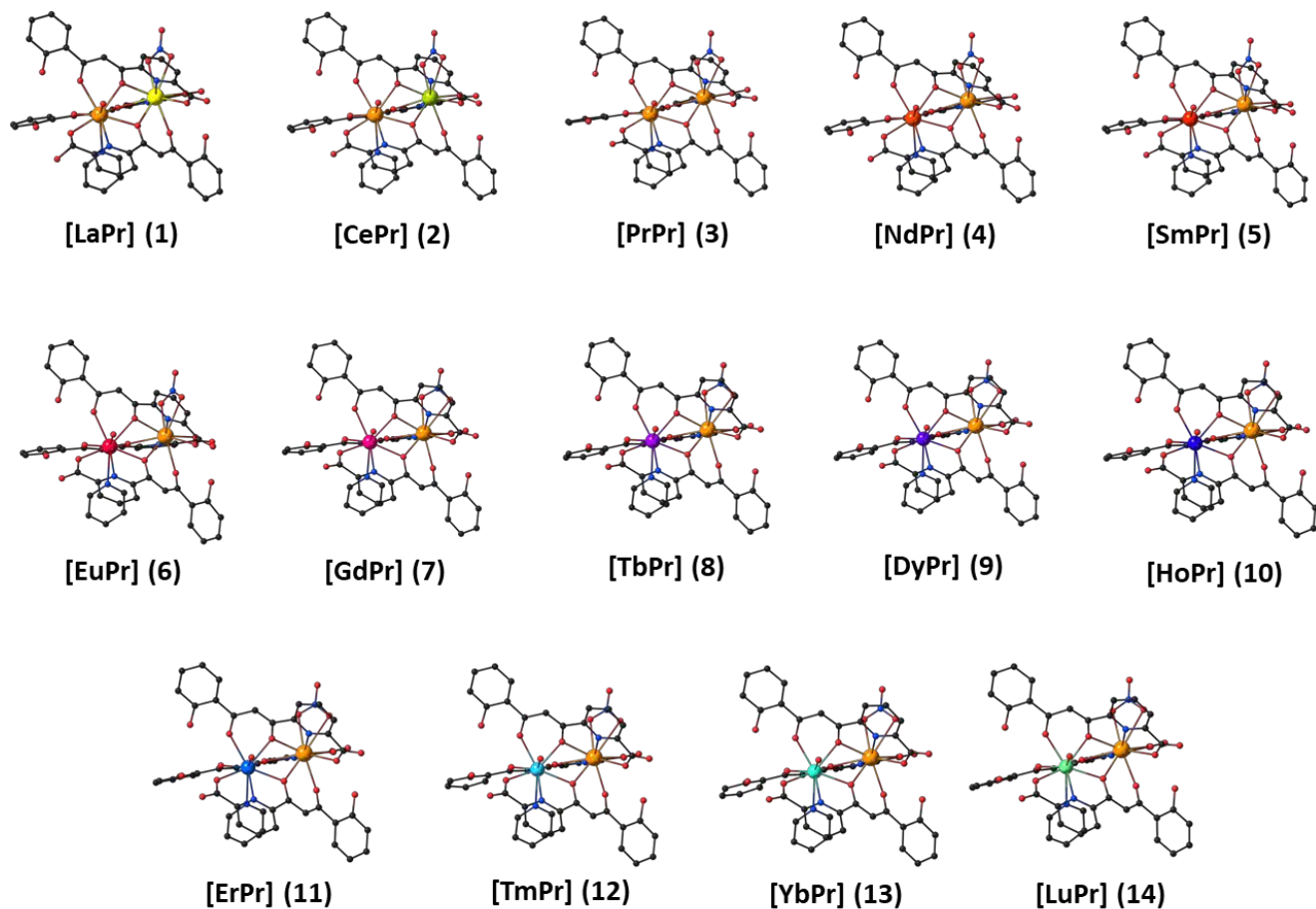
Figure 1. Representation of the anionic complexes in compounds **1**-**14**, with type A configuration for **1** and **2**, and type B distribution for **4**-**14**. Pr, C, N and O atoms are shown in orange, grey, blue and red, respectively. The rest of Ln atoms are represented from yellow (La) to light green (Lu). H atoms are not shown for clarity.

The nature of the cation occupying each site depends on the ionic radius of the accompanying lanthanide ion in the [LnPr] moiety. Thus, ideally, for Ln with ionic radii larger than that of Pr (Ln = La, Ce), coordination site 2 is expected to be occupied by Ln, which favors longer coordination bonds, while the praseodymium cation would be located in site 1 (Scheme 1, type A; Figure 1, compounds **1** and **2**). On the contrary, for the cases where Ln is heavier than Pr (Ln

= Nd to Lu), site 2 is occupied by the praseodymium cation, which exhibits the largest ionic radius of the metallic pair (Scheme 1, type B; Figure 1, compounds **4** - **14**). The smaller size of the accompanying Ln favors its encapsulation in site 1, more suited to promote shorter coordination bonds. In order to confirm this trend in the solid state, the sum of the bond distances between the oxygen atoms from HL^{2-} and the lanthanide ions in each [LnPr] compound, Σd(Ln-O) and Σd(Pr-O), were evaluated and compared for each structure of the series (Table S3-S5; Figure 2, left). The graphic clearly shows the difference between both type A and B systems, separated by compound **3** [PrPr]. The Σd(Pr-O) parameter obtained for compounds **4-14** (type B, with Pr^{III} in site 2) is rather constant, oscillating only between 14.9965(109) and 15.0472(118) Å, and being very close to that obtained for [PrPr] in site 2 (Σd(Pr-O) = 15.03 Å). This strongly suggests that Pr^{III} is inserted in this site for all type B compounds. In contrast, Σd(Ln-O) in this part of the series shows a smooth decrease, from 14.695(18) for [NdPr] (**4**) down to 14.055(37) for [LuPr] (**14**), in good agreement with the decrease of ionic radii of Ln^{III}.[18] This observation underscores that for compounds **4-14**, site 1 is certainly occupied by the varying Ln^{III} cation. In fact, the decay of Σd(Ln-O) along isostructural series of lanthanide complexes has been shown previously to follow a quadratic decrease as a function of the number of f electrons.[34] This decay can be used to evaluate the lanthanide contraction considering the Slater's model.[35] Thus, for a sum of m bond distances (S_m), the model yields a relationship [Eq. 1] where $S_{m\mathbf{L}}$ is defined as the sum of the atomic radii of the m donor atoms involved, r_0 and Z_0^* are the ionic radius and effective nuclear charge of La^{III}, n is the number of f electrons and k is the screening constant for one 4f electron.

$$S_m(n) = S_{m\mathbf{L}} + mr_0 - \left[\frac{mr_0(1-k)}{Z_0^*}\right]n + \left[\frac{mr_0(1-k)^2}{(Z_0^*)^2}\right]n^2 = a + bn + cn^2 \qquad (1)$$
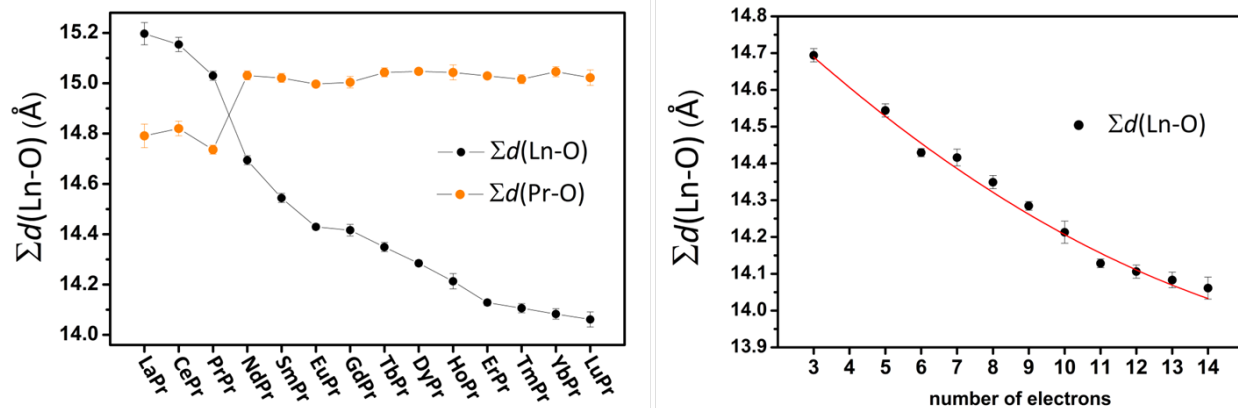
Figure 2. Left: Graph of Σd(Ln-O) and Σd(Pr-O) versus the Ln^{III} participating in each compound of the series, considering the O atoms of the HL^{2-} ligands. Right: Graph of Σd(Ln-O) versus the number of 4f electrons for site 1 of type B compounds ([NdPr] to [LuPr]). Solid line is the best weighted fit to the quadratic function described in the text.

Consequently, the data derived from Σd(Ln-O) for compounds **4-14** were satisfactorily fitted to a polynomial equation of second order employing a weighted regression (weighting regression factor of σ^{-2}) with the following best-fit parameters: $a = 14.96(4)$, $b = -0.099(9)$ and $c = 0.0023(6)$ with $R^2 = 0.9802$ (Figure 2, right). These parameters were used to estimate the screening constant k extracted from Eq. 1 as $k = 1 + Z_0^* c/b$. Considering $Z_0^* = 15.42$,[36] the value obtained, $k = 0.64$, is very close to the commonly accepted value for the screening constant of f-orbitals (0.69) and similar to the number obtained for other reported Ln series.[22, 35] The good agreement obtained for the screening constant parameter also corroborates the occupancy of site 1 by the accompanying Ln cation within this range of compounds.

The values obtained for Σd(Ln-O) and Σd(Pr-O) in compounds **1** and **2** (type A) have been evaluated considering Ln^{III} in site 2 and Pr^{III} in site 1. As expected, the sum of the bond distances in the latter are smaller than in the former. However, the values obtained for Σd(Pr-O)

(14.791(47) and 14.82(29) Å for **1** and **2**, respectively) are slightly above the value observed in

[PrPr] for site 1 (14.736(18) Å), indicating that in this case this cavity could be partially occupied

by the bigger cations La^{III} and Ce^{III}, respectively. These results are not surprising, taking into

account that the difference of ionic radii (Δr) of these ions and Pr^{III} is rather small, limiting here

the selectivity of the distribution of the Ln ions. In order to further assess the metallic

arrangement in these compounds, each crystal structure was refined considering the four possible

metallic distributions: two [LnPr] combinations (type A and type B), [PrPr] and [LnLn]. The

resulting agreement factors (R_1, wR_2, S) and displacement parameters of the two lanthanide ions

(U_{eq}) for each possible metallic arrangement were collected and are shown in Tables S1 and S2.

As expected, similar values were obtained in compounds **1**, **2** and **4** for the four different

distributions, suggesting that the electron density sensed by X-ray diffraction at each site does

not differ sufficiently to support unambiguously one specific composition. This would indicate

that the molecular system cannot clearly distinguish two different Ln ions with Δr < 0.03 Å. In

contrast, for compounds **5**-**14**, type B configuration shows clearly better agreement factors as

well as more realistic displacement parameters for each lanthanide ion of the pair. These results

show that, in the solid state, when the two lanthanide ions have size difference of Δr > 0.06 Å,

the system can selectively place each Ln^{III} inside the expected corresponding cavity. Consistent

with increased size differences (Δr), the refinement parameters for type A [LnPr], [LnLn] and

[PrPr] show systematically worse agreements along the series as we move from compound **5**

([SmPr], Δr = 0.06 Å) to compound **14** ([LuPr], Δr = 0.21 Å).

Mass spectrometry. In order to evaluate the heterometallic nature of compounds **1**-**14** in

solution, a crystalline sample of each system was dissolved in a mixture of MeOH/DMSO and

analyzed by electrospray ionization mass spectrometry (ESI-MS). For all compounds, the spectrogram shows the peak corresponding to the isotopic distribution of the $[LnPr(HL)_2(H_2L)]^+$ moiety, thus confirming the heterometallic nature of each of them. However, in some cases, in agreement with the results obtained in the crystallographic study, additional peaks from the homometallic $[PrPr(HL)_2(H_2L)]^+$ and/or $[LnLn(HL)_2(H_2L)]^+$ moieties are also observed with relative abundances depending on the difference in the ionic radii between Pr^{III} and Ln^{III}. For compounds **12** ([TmPr], $\Delta r = 0.18$ Å), **13** ([YbPr], $\Delta r = 0.19$ Å) and **14** ([LuPr], $\Delta r = 0.21$ Å), the signals for $[PrPr(HL)_2(H_2L)]^+$ and $[LnLn(HL)_2(H_2L)]^+$ are absent or residual (with the exception of $[PrPr(HL)_2(H_2L)]^+$ in compound **13**), while the heterometallic $[LnPr(HL)_2(H_2L)]^+$ moieties virtually dominate the spectra (Figure 3, bottom right, and Figure S2). Similarly, the spectra obtained for compounds **9** ([DyPr], $\Delta r = 0.13$ Å), **10** ([HoPr], $\Delta r = 0.15$ Å) and **11** ([ErPr], $\Delta r = 0.16$ Å) evidence a prominent peak for $[LnPr(HL)_2(H_2L)]^+$, accompanied with very weak signals from $[PrPr(HL)_2(H_2L)]^+$ and $[LnLn(HL)_2(H_2L)]^+$ (Figure 3, bottom left, and Figure S3). For compounds featuring less noticeable size difference (compounds **5-8**, $\Delta r = 0.06\text{-}0.11$), the homometallic moieties are more visible, although still weaker than the $[LnPr(HL)_2(H_2L)]^+$ species (Figure 3, top right, and Figure S4). As previously observed in other [LnLn'] analogues,[23] these results suggest a degree of scrambling of the lanthanide ions in solution, thus reducing the selectivity. This could be facilitated by the dissociation of the H_2O, py and NO_3^- terminal ligands, and is in agreement with DFT calculations (see below). However, the gradual decrease in importance of the $[PrPr(HL)_2(H_2L)]^+$ and $[LnLn(HL)_2(H_2L)]^+$ species along the series confirms that, in solution, the selectivity is also higher when the difference between the ionic radii of the two concerned lanthanide ions is larger. The presence of even more noticeable signals from homometallic moieties observed in the mass spectrograms of **1**, **2** and **4** ($\Delta r = 0.03$,

0.02 and 0.03, respectively, , top left, and) agrees with this trend, although these species could also be present in the original crystalline sample (see above).
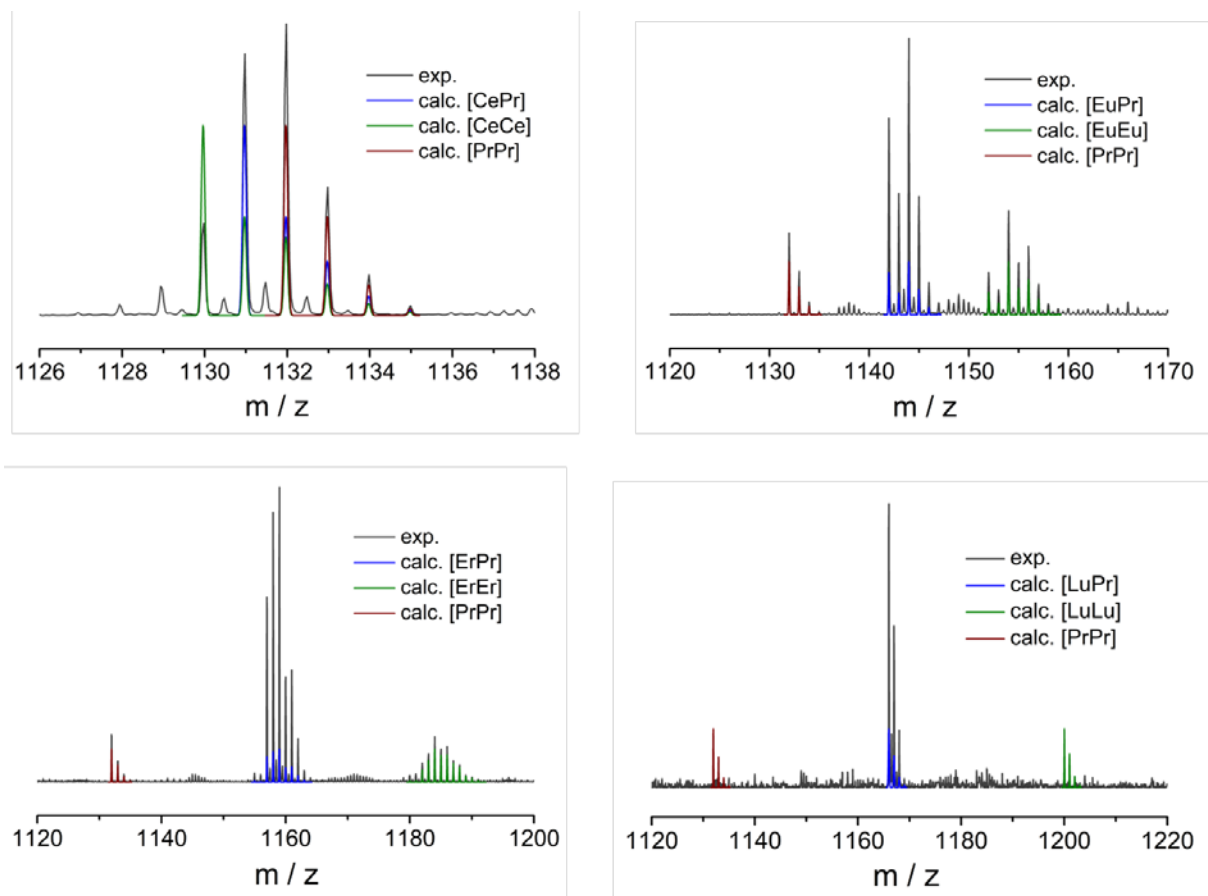

Figure 3. Selected region of the experimental (grey line) ESI-MS spectra of compounds **2** ([CePr], top left), **6** ([EuPr], top right), **11** ([ErPr], bottom left) and **14** ([LuPr], bottom right), together with the calculated signals corresponding to [LnPr] (blue line), [LnLn] (green line) and [PrPr] (red line).

Magnetic properties. Being able to vary at will the metal composition of polymetallic complexes can be very useful for the detailed study of magnetic properties, as we have shown in our study of the spin-based quantum gate prototype [CeEr] molecule.[15] Replacing each magnetic

lanthanide ion with a diamagnetic one allowed to determine the behaviour of each qubit of the molecular pair isolated from the other, but in the same environment. In the present [PrLn] series, the most interesting molecule in terms of magnetic properties is arguably the [PrDy] compound **9**, due to the large unquenched orbital angular momentum of the Dy(III) and the very likely associated observation of slow relaxation of its magnetization.[10, 37] To illustrate the interest of the site composition control, we have thus studied the static and dynamic magnetic properties of both [PrDy] (**9**) and [PrLu] (**14**) compounds. First, the temperature dependence of the equilibrium magnetic susceptibilities of both compounds was determined through *dc* magnetization measurements as well as (low temperatures) zero-field *ac* susceptibility measurements at 15 Hz (Figure 4). These are in good agreement with the chemical composition of both heterometallic compounds. The χT value of **9** is 16.64 cm^{3}mol^{-1}K at 300 K, slightly higher than the sum of expected values for one Dy(III) ion (^{6}H$_{15/2}$, $g = 4/3$, 14.17 cm^{3}mol^{-1}) and one Pr(III) ion (^{3}H$_4$, $g = 4/5$, 1.60 cm^{3}mol^{-1}), and decreases gradually below *ca.* 150 K, likely as a consequence of the thermal depopulation of energy levels split by the crystal field of both ions. A semi-logarithmic plot shows that the data tend towards a plateau of, *ca.* 12.6 cm^{3}mol^{-1}K at 2 K. For **14**, the χT value of 1.71 cm^{3}mol^{-1}K at 300 K is slightly higher than expected for one Pr(III) ion, and decreases below *ca.* 150 K, first gradually and then more rapidly, to reach 0.10 cm^{3}mol^{-1}K at 1.8 K. A semi-logarithmic plot shows that the data tend towards zero. Magnetization *vs.* field data at 2 K are in line with the susceptibility data. For **9**, a fast increase up to *ca.* 6 $N_A\mu_B$ at 2 T is observed, followed by a further slower and quasi-linear increase at higher fields, which most likely is primarily associated with the Pr(III) ion. Indeed, in the case of **14** a linear increase is observed up to the highest accessible field of 5 T, which can be ascribed to the population of higher energy sub-levels. A first conclusion is that the properties of **9** are not

affected by any exchange interaction, consistent with the typically very weak nature of these among lanthanide ions and the vanishing spin density remaining at the Pr(III) ion in **14** at low temperatures. Then, substracting the data of **14** from those of **9** indirectly gives an estimate of the magnetic properties of the isolated Dy(III) ion in **9** (Figure 4), with a value of $M = 6.16$ $N_A\mu_B$ at 5 T and a low temperature χT plateau of 12.67 cm^{3}mol^{-1}K at 2 K in good agreement with each other. The availability of such data would be particularly useful to quantify the anisotropy of the sole Dy(III) ion in **9**, although this is beyond the scope of this work.
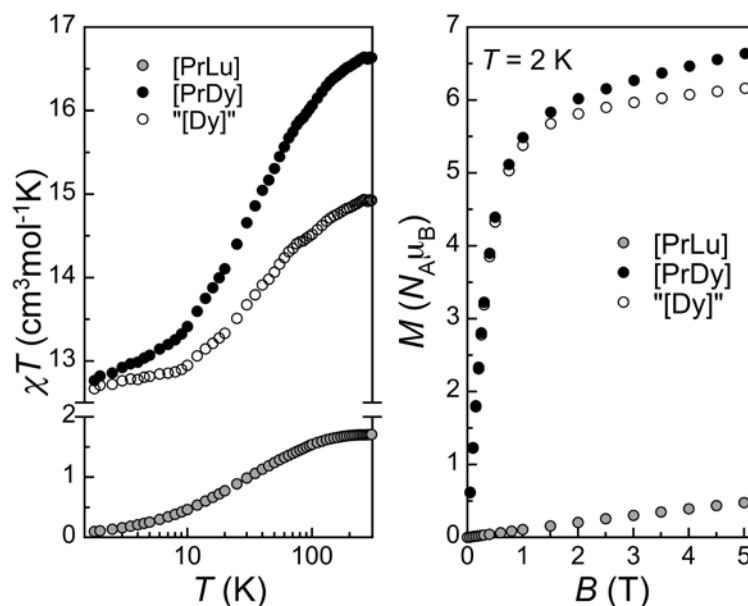

Figure 4. Static magnetic properties of compounds **9** and **14**. Left: semi-logarithmic plot of the temperature dependence of the χT product, χ being the molar paramagnetic susceptibility. Right: Field dependence of the magnetization (M) at 2 K.

To evaluate the potential single-molecule magnet behaviour of **9**, its magnetization dynamics were investigated through isothermal *ac* susceptibility measurements at variable frequency. In

zero *dc* field, an out-of-phase signal is detected, indicative of slow relaxation of magnetization (Figure S6). This relaxation however has two distinct components, one dominant faster mode with a characteristic frequency above the highest accessible with our set-up (10 kHz), and a minor, slower mode clearly visible at lower temperatures, in form of a hump within the studied frequency window. To extract the characteristic time of this slow relaxation mode, a generalized Debye model was fit to the out-of-phase data considering the sum of two components and fixing the fast component τ to 3.18×10^{-6} s (see Table S6). This was not possible at higher temperatures and then only one characteristic time was derived. Under applied *dc* fields, the relaxation becomes slower, and maxima of the out-of-phase signal are observed in our frequency window (Figure 5, top). In these conditions, only one relaxation mode is detected, and all further data were analyzed with a single generalized Debye model to extract the corresponding characteristic times for the various *dc* fields (at 1.8 K, Table S7) and temperatures (at 500 and 1000 Oe, Figure S7 and S8, Table S6). Compound 14 was also studied under the same conditions. The absence of any out-of-phase susceptibility (Figure S9) supports the hypothesis that the slow magnetization dynamics observed for **9** must be ascribed to the Dy(III) ion. The fast relaxation mode of [PrPr] (**9**) present in zero field and its cancellation upon applying a *dc* field suggests the presence of fast quantum tunnelling of magnetization, with τ_{QTM} likely of the order of 10^{-5} s.
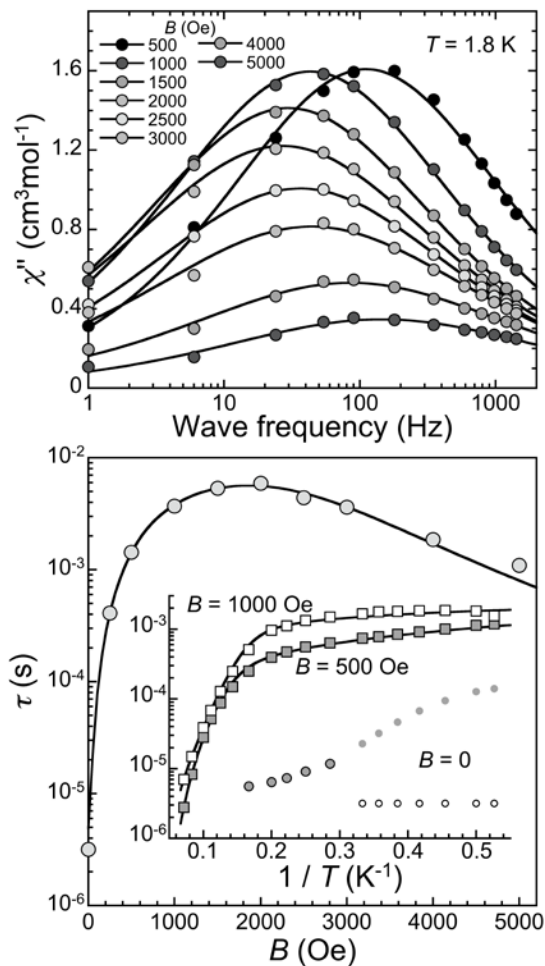
Figure 5. *ac* magnetic susceptibility of compound **9**. Top: Frequency-dependence of the out-of-phase susceptibility at 1.8 K at the indicated applied *dc* fields. Full lines are the best-fit of the generalized Debye model to the data. Bottom: Field dependence of the characteristic spin-lattice relaxation time τ at 1.8 K. The inset shows the temperature dependence of τ at the indicated applied *dc* field, evidencing the two components at $B = 0$. Full lines are fits to an expression including the relevant relaxation modes (see text).

At 1.8 K, the field dependence of the spin relaxation time τ of **9** shows a non-monotonous variation (Figure 5, bottom). The increase observed at low fields is likely due to the reduced

effect of spin-spin and spin-nuclei processes upon increasing the *dc* field, while the decrease at fields above 0.2 T likely results from the then dominant spin phonon direct mechanism, which is $\propto B^4$. At 500 and 1000 Oe, the temperature dependence of τ clearly exhibits a strong thermal activation above 5 K, and a steady decrease below (Figure 5, inset). To gain further insights on the relaxation processes at work avoiding over-parameterization, the expression

$$\tau^{-1} = AB^4T + D_1/(1 + D_2B^2) + cst$$

was first fit to the field dependence of the spin relaxation time τ at 1.8 K (Table S8), allowing for a separate estimation of the direct process with $A = 1.0 \times 10^{-4}$ s. Then, the expression

$$\tau^{-1} = AB^4T + \tau_0^{-1}exp(-U_{eff}/k_BT) + CT^n$$

, that includes respectively the temperature dependent direct, Orbach and Raman relaxation mechanisms, was fit to the temperature dependence of τ for **9** at 500 and 1000 Oe, fixing n at the expected value of 9 for a Kramers ion (Table S9). The derived parameters $\tau_0 = 2.15 \times 10^{-6}$ s, U_{eff} = 53 K and $C = 1.7 \times 10^{-6}$ s^{-1}K^{-9} at 1000 Oe and $\tau_0 = 2.52 \times 10^{-6}$ s, U_{eff} = 53 K and $C = 1.28 \times 10^{-5}$ s^{-1}K^{-9} at 500 Oe suggest both Orbach and Raman mechanisms are involved in the thermal activation of the relaxation and are thus difficult to accurately estimate.

One of the great benefits of the controlled site composition in polynuclear lanthanide complexes is that it provides a means to study the exchange interaction between lanthanide ions. As mentioned above, this interaction is rather weak, which makes it hard to trace using standard magnetic measurements. The vanishing spin density of Pr at low temperatures reduces the relevance of this problem in this series of compounds. However, this important issue has required to study analogues containing the lanthanide of interest next to a diamagnetic anion within isolated molecules, diluted inside a fully diamagnetic crystalline matrix.[38] It would be

better to use pure heterodimetallic compounds with the desired composition, and therefore the current system holds great potential in this respect.

DFT studies. In order to rationalize the selectivity of the metallic distribution and the stability of type A or type B configurations along the [LnPr] series, compounds **1** (LaPr), **7** (GdPr) and **14** (LuPr) were investigated by DFT-based methods. The structures determined in the solid state by single crystal X-ray diffraction were computed as anionic complexes with formula $[LnPr(HL)_3(NO_3)(py)(H_2O)]^-$. The selectivity in solution was evaluated by studying these ions in the absence of the nitrate, pyridine and H_2O terminal ligands, thus using the moiety $[LnPr(HL)_3]^-$. For both, solid state and solution systems, the energy difference between both heterometallic configurations (ΔE) in each compound was calculated, considering type A as the most stable one for compound **1**, and type B for compounds **7** and **14**. The results shown in Table 2 demonstrate that in the solid state, each expected configuration is the most stable one, and that this preference is bigger for larger differences of ionic radii (Δr). In fact, the small value of ΔE obtained for **1** agrees with the results obtained in the crystallographic study where no significant differences where observed between type A and type B configurations in the structural refinement (Table S1). Consistent with the experiment, the energy differences obtained without the terminal ligands (solution) are smaller than in the solid state. This feature, which had been noticed previously for [SmPr],[23] confirms the reduced selectivity in solution, perhaps due to the absence of these ligands. This decrease of selectivity is particularly important in compound **1**, for which the preference for type A is no longer observed (-0.97 kcal mol^{-1}). As expected, the selectivity for compounds **7** and **14** increases with Δr.

The description of chemical systems with unpaired number of electrons (open-shell) is a source of contention within the computational chemistry community. [39, 40] Our group studied similar dinuclear systems previously using the BP86 functional[23] obtaining results in agreement with the experimental trend. However, in order to confirm the accuracy of the employed DFT-functional (BP86), we have used a different DFT-functional (B3LYP) from which we obtained the same trend in the selectivity (Table 2). On the other hand, relativistic Spin-Orbit calculations were also used to corroborate that scalar relativistic effects describe the system correctly. The results depicted in row 3 of Table 2 present minor differences with respect to the scalar relativistic ZORA methodology.

Table 2. Calculated energy differences (ΔE) for compounds **1**, **7** and **14** in solid state and solution in relation with the ionic radii differences (Δr).

ΔE [kcal mol^{-1}]	*Solid State*			*Solution (No terminal ligands)*		
	1 ([LaPr] A)	**7** ([GdPr] B)	**8** ([LuPr] B)	**1** ([LaPr] A)	**7** ([LaPr] B)	**14** ([LaPr] B)
BP86	0.46	4.78	8.12	-0.97	2.07	2.27
B3LYP	2.14	3.20	6.61	-0.90	0.80	2.29
Spin-Orbit (BP86)	0.56	3.92	7.81	-0.92	1.89	2.27
Δr [Å]	0.05	0.095	0.205	0.05	0.095	0.205

CONCLUSIONS

The complete series of [LnPr] complexes reported here represents an ideal showcase of the potential and limits of the (Hpy)[LnLn'(HL)$_3$(NO$_3$)(py)(H$_2$O)] system to promote heterometallic molecular entities. The results found from a comprehensive crystallographic study evidence that when the difference between the ionic radii of the two Ln ions is small ($\Delta r < 0.03$ Å), the system cannot fully discriminate them. In contrast, when the difference is larger than 0.06 Å, the lanthanides are selectively distributed in the two different cavities of the molecular entity. This selectivity is effectively maintained in solution for large differences of ionic radii ($\Delta r > 0.16$ Å), since virtually only signals related to the heterometallic moiety are detected in MS spectrometry. However, the scrambling of the lanthanide ions in solution surface when such difference is reduced, deriving in a mixture of hetero- and homometallic moieties, the latter with a higher influence for smaller values of Δr. The experimental results are consistent with the DFT calculations, which confirmed the selectivity limits both in the solid state and solution. Of the different pure heterometallic systems presented, the [DyPr] derivative was found to exhibit the characteristics of a single-molecule magnet. The absence of magnetization slow dynamics in the [LuPr] analogue suggests that the single molecule magnet behavior arises purely from the Dy(III) ion. The study of this new series thus shows that this molecular system can promote a vast number of pure [LnLn'] combinations, opening the possibility to further tune and exploit their magnetic and optical properties.

ASSOCIATED CONTENT

Supporting Information.

The Supporting Information is available free of charge on the ACS Publications website at DOI: XXXX. Additional structural data for compounds **1**, **2**, **4**, **6**-**14** and magnetic data for compounds **9** and **14** (PDF). CCDC XXXX-XXXX contain the supplementary crystallographic data of the compounds reported in this paper, which can be obtained free of charge upon request. All computational data is available in the ioChem-BD repository[33] and can be accessed via http://dx.doi.org/10.19061/iochem-bd-1-64.

AUTHOR INFORMATION

Corresponding Author

*E-mail for G. A.: guillem.aromi@qi.ub.es

Author Contributions

The manuscript was written through contributions of all authors. All authors have given approval to the final version of the manuscript.

Notes

The authors declare no competing financial interest.

REFERENCES

[1] Huang, C. *Rare earth coordination chemistry*, John Wiley & Sons, Singapore, **2010**.

[2] Bettencourt-Dias, A. d. *Luminescence of lanthanide ions in coordination compounds and nanomaterials*, John Wiley & Sons, Chichester, **2014**.

[3] Layfield, R. A.; Murugesu, M. *Lanthanides and actinides in molecular magnetism*, Wiley-VHC, Weinheim, **2015**.

[4] Zheng, Z. Recent development in clusters of rare earths and actinides: chemistry and materials. *Structure and Bonding* **2017**, *173*, 1-50.

[5] Jinnai, K.; Kabe, R.; Adachi, C. A near-infrared organic light-emitting iode based on an Yb(III) complex synthesized by vacuum co-deposition. *Chem. Commun*. **2017**, *53*, 5457-5460.

[6] Amoroso, A. J.; Pope, S. J. A. Using lanthanide ions in molecular bioimaging. *Chem. Soc. Rev*. **2015**, *44*, 4723-4742.

[7] a) Sibille, R.; Mazet, T.; Malaman, B.; François, M. A metal-organic framework as attractive cryogenic magnetorefrigerant. *Chem. Eur. J*. **2012**, *18*, 12970-12973. b) Lorusso, G.;

Palacios, M. A.; Nichol, G. S.; Brechin, E. K.; Roubeau, O.; Evangelisti, M. Increasing the dimensionality of cryogenic molecular coolers: Gd-based polymers and metal-organic frameworks. *Chem. Commun*. **2012**, *48*, 7592-7594.

[8] Woodruff, D. N.; Winpenny, R. E. P.; Layfield, R. A. Lanthanide single-molecule magnets. *Chem. Rev*. **2013**, *113*, 5110-5148.

[9] Ishikawa, N.; Sugita, M.; Ishikawa, T, Koshihara, S.; Kaizu, Y. Lanthanide double-decker complexes functioning as magnets at the single-molecular level. *J. Am. Chem. Soc*. **2003**, *125*, 8694-8695.

[10] a) Guo, F.-S.; Day, B. M.; Chen, Y. C.; Tong, M.-L.; Mansikkamäki, A.; Layfield, R. A. A dysprosium metallocene single-molecule magnet functioning at the axial limit. *Angew. Chem. Int. Ed*. **2017**, *56*, 11445-11449. b) Goodwin, C. A. P.; Ortu, F.; Reta, D.; Chilton, N. F.; Mills, D. P. *Nature* **2017**, *548*, 439-442.

[11] Zhou, J.; Liu, Q.; Feng, W.; Sun, Y.; Li, F. Upconversion luminescent materials: advances and applications. *Chem. Rev*. **2015**, *115*, 395-465.

[12] Guillou, O.; Daiguebonne, C.; Calvez, G.; Bernot, K. A long journey in lanthanide chemistry: from fundamental crystallogenesis studies to commercial anticounterfeiting taggants. *Acc. Chem. Res*. **2016**, *49*, 844-856.

[13] Mamedov, I.; Parac-Vogt, T. N.; Logothetis, N. K.; Angelovski, G. Synthesis and characterization of dinuclear heterometallic lanthanide complexes exhibiting MRI and luminescence response. *Dalton Trans*. **2010**, *39*, 5721-5727.

[14] a) Luis, F.; Martínez-Pérez, M. J.; Aguilà, D.; Roubeau, O.; Zueco, D.; Alonso, P. J.; Evangelisti, M.; Camón, A.; Sesé, J.; Barrios, L. A.; Aromí, G. Molecular prototypes for spin-based CNOT and SWAP quantum gates. *Phys. Rev. Lett*. **2011**, *107*, 117203(1-5). b) Baldoví, J. J.; Rosaleny, L. E.; Ramanchandran, V.; Christian, J.; Dalal, N. S.; Clemente-Juan, J. M.; Yang, P.; Kortz, U.; Gaita-Ariño, A.; Coronado, E. Molecular spin qubits based on lanthanide ions encapsulated in cubic polyoxopalladates: design criteria to enhance coherence. Inorg. Chem. Front. 2015, 2, 893-897. c) Pedersen, K. S.; Ariciu, A.-M.; McAdams, S.; Weihe, H.; Bendix, J.; Tuna, F.; Piligkos, S. Toward molecular 4f single-ion magnet qubits. *J. Am. Chem. Soc*. **2016**, *138*, 5801-5804.

[15] Aguilà, D.; Barrios, L. A.; Velasco, V.; Roubeau, O.; Repollés, A.; Alonso, P. J.; Sesé, J.; Teat, S. J.; Luis, F.; Aromí, G. Heterometallic [LnLn'] lanthanide complexes: towards a chemical design of two-qubit molecular spin quantum gates. *J. Am. Chem. Soc*. **2014**, *136*, 14215-14222.

[16] a) Costes, J.-P.; Nicodème, F. Unequivocal synthetic pathway to heterodinuclear (4f,4f') complexes: magnetic study of relevant (Ln^{III}, Gd^{III}) and (Gd^{III}, Ln^{III}) complexes. *Chem. Eur. J*. **2002**, *8*, 3442-3447. b) Costes, J.-P.; Dahan, F.; Nicodème, F. Structure-based description of a step-by-step synthesis of homo- and heterodinuclear (4f,4f') lanthanide complexes. *Inorg. Chem*. **2003**, *42*, 6556-6563. c) Faulkner, S.; Pope, S. J. A. Lanthanide-sensitized lanthanide luminescence: terbium-sensitized ytterbium luminescence in a trinuclear complex. *J. Am. Chem. Soc*. **2003**, *125*, 10526-10527. d) Zhu, P.; Pan, N.; Li, R.; Dou, J.; Zhang, Y.; Cheng, D. Y. Y.; Wang, D.; Ng, D. K. P.; Jiang, J. Electron-donating alkoxy-group-driven synthesis of heteroleptic tris(phthalocyaninato) lanthanide(III) triple-deckers with symmetrical molecular structure. *Chem. Eur. J*. **2005**, *11*, 1425-1432. e) Lewis, D. J.; Glover, P. B.; Solomons, M. C.;

Pikramenou, Z. Purely heterometallic lanthanide(III) macrocycles through controlled assembly of disulfide bonds for dual color emission. *J. Am. Chem. Soc*. **2011**, *133*, 1033-1043. f) Sato, R.; Suzuki, K.; Sugawa, M.; Mizuno, N. Heterodinuclear lanthanoid-containing polyoxometalates: stepwise synthesis and single-molecule magnet behavior. *Chem. Eur. J*. **2013**, *19*, 12982-12990. g) Lan, Y.; Klyatskaya, S.; Ruben, M.; Fuhr, O.; Wernsdorfer, W.; Candini, A.; Corradini, V.; Lodi Rizzini, A.; del Pennino, U.; Troiani, F.; Joly, L.; Klar, D.; Wende, H.; Affronte, M. Magnetic interplay between two different lanthanides in a tris-phthalocyanato complex: a viable synthetic route and detailed investigation in the bulk and on the surface. *J. Mater. Chem. C* **2015**, *3*, 9794-9801.

[17] a) Natrajan, L. S.; Villaraza, A. J. L.; Kenwright, A. M.; Faulkner, S. Controlled preparation of a heterometallic lanthanide complex containing different lanthanides in symmetrical binding pockets. *Chem. Commun*. **2009**, 6020-6022. b) Placidi, M. P.; Villaraza, A. J. L.; Natrajan, L. S.; Sykes, D.; Kenwright, A. M.; Faulkner, S. Synthesis and spectroscopic studies on azo-dye derivatives of polymetallic lanthanide complexes: using diazotization to link metal complexes together. *J. Am. Chem. Soc*. **2009**, *131*, 9916-9917. c) Tilney, J. A.; Sørensen, T. J.; Burton-Pye, B. P.; Faulkner, S. Self-assembly between dicarboxylate ions and a binuclear europium complex: formation of stable adducts and heterometallic lanthanide complexes. *Dalton Trans*. **2011**, *40*, 12063-12066.

[18] D'Angelo, P.; Zitolo, A.; Migliorati, V.; Chillemi, G.; Duvail, M.; Vitorage, P.; Abadie, S.; Spezia, R. Revised ionic radii of lanthanoid(III) ions in aqueous solution. *Inorg. Chem*. **2011**, *50*, 4572-4573.

[19] a) André, N.; Scopelliti, R.; Hopfgartner, C.; Piguet, C.; Bünzli, J.-C. G. Discriminating between lanthanide ions: self-assembly of heterodimetallic triple-stranded helicates. *Chem. Commun.* **2002**, 214-215. b) André, N.; Jensen, T. B.; Scopelliti, R.; Imbert, D.; Elhabiri, M.; Hopfgartner, G.; Piguet, C.; Bünzli, J.-C. G. Supramolecular recognition of heteropairs of lanthanide ions: a step toward self-assembled bifunctional probes. *Inorg. Chem.* **2004**, *43*, 515-529.

[20] Floquet, S.; Borkovec, M.; Bernardinelli, G.; Pinto, A.; Leuthold, L.-A.; Hopfgartner, G.; Imbert, D.; Bünzli, J.-C. G.; Piguet, C. Programming heteropolymetallic lanthanide helicates: thermodynamic recognition of different metal ions along the strands. *Chem. Eur. J.* **2004**, *10*, 1091-1105.

[21] Artizzu, F.; Quochi, F.; Marchio, L.; Correja, R. F.; Saba, M.; Serpe, A.; Mura, A.; Mercuri, M. L.; Bongiovanni, G.; Deplano, P. Ln_3Q_9 as a molecular framework for ion-size-driven assembly of heterolanthanide (Nd, Er, Yb) multiple near-infrared emitters. *Chem. Eur. J.* **2015**, *21*, 3882-3885.

[22] Aguilà, D.; Barrios, L. A.; Velasco, V.; Arnedo, L.; Aliaga-Alcalde, N.; Menelaou, M.; Teat, S. J.; Roubeau, O.; Luis, F.; Aromí, G. Lanthanide contraction within a series of asymmetric dinuclear [Ln_2] complexes. *Chem. Eur. J.* **2013**, *19*, 5881-5891.

[23] Gónzalez-Fabra, J.; Bandeira, N. A. G.; Velasco, V.; Barrios, L. A.; Aguilà, D.; Teat, S. J.; Roubeau, O.; Bo, C.; Aromí, G. Thermodynamic stability of heterometallic [LnLn'] complexes: synthesis and DFT studies. *Chem. Eur. J.* **2017**, *23*, 5117-5125.

[24] Aguilà, D.; Barrios, L. A.; Luis, F.; Repollés, A.; Roubeau, O.; Teat, S. J.; Aromí, G. Synthesis and properties of a family of unsymmetric dinuclear complexes of Ln[III] (Ln = Eu, Gd, Tb). *Inorg. Chem.* **2010**, *49*, 6784-6786.

[25] SAINT and SADABS, Bruker AXS Inc., Madison, Wisconsin, USA.

[26] Sheldrick, G. M. *SHELXT* - Integrated space-group and crystal-structure determination. *Acta Cryst. Sect. A* **2015**, *71*, 3-8

[27] Sheldrick, G. M. Crystal structure refinement with SHELXL. *Acta Cryst. Sect. C* **2015**, *71*, 3-8.

[28] Becke, A. D. Density-functional exchange-energy approximation with correct asymptotic behaviour. *Phys. Rev. A* **1988**, *38*, 3098-3100.

[29] a) Perdew, J. P. Density-functional approximation for the correlation energy of the inhomogeneous electron gas. *Phys. Rev. B* **1986**, *33*, 8822-8824. b) Perdew, J. P. Density-functional approximation for the correlation energy of the inhomogeneous electron gas. *Phys. Rev. B* **1986**, *34*, 7406-7406.

[30] a) Becke, A.D. Density-functional thermochemistry. III. The role of exact exchange. *J. Chem. Phys.* **1993**, *98*, 5648-5652. b) Lee, C.; Yang, W.; Parr, R.G. Development of the Colle-Salvetti correlation-energy formula into a functional of the electron density. *Phys. Rev. B* **1988**, *37*, 785-789.

[31] a) Van Lenthe, E.; Baerends, E. J. Optimized Slater-type basis sets for the elements 1–118. *J. Comput. Chem.* **2003**, *24*, 1142-1156; b) Van Lenthe, E.; Baerends, E. J.; Snijders, G. Relativistic regular two-component Hamiltonians. *J. Chem. Phys.* **1993**, *99*, 4597-4610.

[32] Becke, A.D. A multicenter numerical integration scheme for polyatomic molecules. *J. Chem. Phys*. **1988**, *88*, 2547-2553.

[33] Álvarez-Moreno, M.; de Graaf, C.; López, N.; Maseras, F.; Poblet, J. M.; Bo, C. Managing the computational chemistry big data Problem: the ioChem-BD Platform. *J. Chem. Inf. Model*. **2015**, *55*, 95-103.

[34] Quadrelli, E. A. Lanthanide contraction over the 4f series follows a quadratic decay. *Inorg. Chem*. **2002**, *41*, 167-169.

[35] Seitz, M.; Oliver, A. G.; Raymond, K. N. The lanthanide contraction revisited. *J. Am. Chem. Soc*. **2007**, *129*, 11153-11160.

[36] Clementi, E.; Raimondi, D. L.; Reinhardt, W. P. Atomic screening constants from SCF functions. II. Atoms with 37 to 86 electrons. *J. Chem. Phys*, **1967**, *47*, 1300-1307.

[37] Zhang, P.; Guo, Y.-N.; Tang, J. Recent advances in dysprosium-based single molecule magnets: structural overview and synthetic strategies. *Coord. Chem. Rev*. **2013**, *257*, 1728-1763.

[38] Giansiracusa, M. J.; Moreno-Pineda, E.; Hussain, R.; Marx, R.; Martínez Prada, M.; Neugebauer, P.; Al-Badran, S.; Collison, D.; Tuna, F.; van Slageren, J.; Carretta, S.; Guidi, T.; McInnes, E. J. L.; Winpenny, R. E. P.; Chilton, N.F. Measurement of magnetic exchange in asymmetric lanthanide dimetallics: toward a transferable theoretical framework. *J. Am. Chem. Soc*. **2018**, *140*, 2504-2513.

[39] Jacob, C. R.; Reiher, M. Spin in density-functional theory. *Int. J. Quantum Chem*. **2012**, *112*, 3661–3684.

[40] Ferbinteanu, M.; Stroppa, A.; Scarrozza, M.; Humelnicu, I.; Maftei, D.; Frecus, B.; Cimpoesu, F. On the density functional theory treatment of lanthanide coordination compounds: a comparative study in a series of Cu−Ln (Ln = Gd, Tb, Lu) binuclear complexes. *Inorg. Chem.* **2017**, *56*, 9474−9485.